Numerical Simulation of Semi-Crystalline Nylon 6: Elastic Constants of Crystalline and Amorphous Parts

K. J. Hsia[1], Y.-B. Xin and L. Lin*[2]

Department of Theoretical and Applied Mechanics
University of Illinois at Urbana-Champaign, Urbana, IL 61801

*Department of Mechanical Engineering
Massachusetts Institute of Technology, Cambridge, MA 02139

November, 1992

1 To whom correspondence and proofs should be sent. Tel: (217)333-2321.
2 Current address: Du Pont Marshall R&D Lab, Philadelphia, PA 19146.

ABSTRACT

The elastic responses of crystalline and amorphous parts in semi-crystalline nylon 6 are determined by computer simulation using the finite element method. Semi-crystalline nylon 6 is modelled as a composite consisting of alternating layers of lamellar crystals and amorphous regions. Full morphological details identified by Lin and Argon[1] in their highly textured nylon 6 bulk samples are incorporated in the model. An optimization scheme is employed to systematically search for the individual components' elastic constants which give rise to a composite elastic behavior as that measured by Lin and Argon[1]. A two-dimensional plane strain finite element analysis is performed to evaluate the composite elastic behavior for given set of constituents' elastic constants. The resulted elastic constants of semi-crystalline nylon 6 for the optimized values of crystalline and amorphous elastic properties are within 6% average error with the experimental data. The computations also reveal that high stress concentration exists in the crystalline region. Therefore, experimental measurements of plastic resistance may represent a significant underestimate of the intrinsic critical resolved shear strength of polymer crystals.

I. Introduction

Mechanical properties of semi-crystalline polymers have been of interests to researchers for decades[1-4], simply because they are parameters of first order importance in characterizing mechanical behaviors of these materials. It is well known that polymers possess anisotropic mechanical properties after a large-deformation process, such as drawing, rolling or compression. The anisotropic macroscopic behaviors can be attributed to the texture or orientation distribution of molecules, developed during the deformation, and the intrinsically different bonding forces between atoms. Along with the new findings concerning their microstructures and morphologies, deformation mechanisms in semi-crystalline polymers are being gradually revealed[5]. Recently, bulk samples of semi-crystalline nylon 6, with dual lattice orientations but in overall orthotropic symmetry and with simple and well defined lamellar morphology in near quasi-crystal perfection, were obtained by plane-strain compression in a deep channel die[1]. Taking advantage of the large size of these samples, a complete set of nine elastic constants of highly textured nylon 6 were measured by a simple mechanical testing technique. Furthermore, different plastic deformation systems in this material were identified, and the corresponding plastic resistances were measured. These macroscopic measurements have provided important information which are useful in obtaining microscopic mechanical properties of both the crystalline and the amorphous components of the material.

In order to accurately interpret and, moreover, predict the elastic and plastic responses of a bulk semi-crystalline polymer of a specific texture and morphology such as those made of spherulites, it is crucial to know the mechanical properties of both crystalline part and amorphous part, in addition to a thorough knowledge of the texture and morphology of the material. Elastic constants of polymer crystals have been estimated according to lattice dynamics theory[6]. An easier but more sophisticated method to calculate elastic constants of polymer crystals with more complicated structures was developed[7] and applied to several semi-crystalline polymers including nylon 6[8]. However, there is very limited experimental information available to verify these theoretical calculations[9-11]. For the amorphous region of semi-crystalline bulk polymers, we know not only very little about their mechanical properties[12], but a fundamental issue on how molecules re-enter into lamellar crystals from which they emerged is still controversial[13].

Despite the insufficiency of information, attempts were made to relate macroscopic measurements to micro-mechanical properties and morphological details of semi-crystalline polymers. An aggregate model, proposed by Ward[14], considers polymers as a random aggregate of anisotropic units. Although this model is in principle only valid for amorphous polymers, it provides a good first approximation of mechanical properties for semi-crystalline polymers[15,16]. On the other hand, Takayanagi model[17] has been widely applied to quantitatively characterize highly oriented semi-crystalline polymers. This model has been generalized to two-dimensional[18] and, recently, three-dimensional[2] cases, and has been further modified to analyze shear behavior[2]. The Takayanagi model[17] recognizes the two-phase nature of semi-crystalline polymers, but it lumps crystalline regions and amorphous regions into blocks joining in series or/and parallel so that it fails to take into account the morphological features of the materials. A different two-phase model suggested by Halpin and Kardos[19,20] showed that the geometry effects and orientation effects of lamellar crystals embedded in amorphous materials can be very critical, and may cause the elastic constants to vary by a factor of ten or more. In a multi-step study of polymers with spherulitic structures, Wang[21-23] calculated elastic constants at three different scales (lamellae, spherulites, and bulk) with detailed considerations of morphology of the materials. One of the principal assumptions he made to make the problem tractable was local transverse isotropy about the radius of spherulites. The composite theories of Hill[24], Hermans[25], and Kroner[26] were applied in Wang's calculations to account for mechanical interactions between the two phases and between individual spherulites. Although an elegant approach, Wang's scheme has not been adopted by others, probably due to its complexity. Nevertheless, it is very difficult to apply Wang's method to evaluate micro-mechanical properties of individual constituents from macroscopic measurements.

The present communication is an attempt to reveal the individual elastic responses of the crystalline part and the amorphous part in nylon 6 by computer simulation using the finite element method. The particular sets of elastic constants for crystalline and amorphous parts which result in the elastic response of the textured nylon 6 are searched through an optimization scheme. The respective elastic constants for crystalline and amorphous parts obtained through this simulation are compared with other people's theoretical and experimental studies. Furthermore, plastic resistance of the material could also be studied in principle for any given morphology once the critical

resolved shear strengths in different slip systems are known.

II. Problem Formulation

Highly textured, semi-crystalline nylon 6 is modeled as a composite consisting of crystalline part and amorphous part, each with its own elastic properties. The objective is to find the set of elastic constants for crystalline and amorphous parts which give rise to the composite elastic behaviors of nylon 6 as that measured by Lin and Argon[1]. The elastic constants of the constituents are systematically guessed through an algorithm to be discussed in the next section, and the composite's elastic response will be calculated and compared with the experimental data until they match each other. The finite element method was used to calculate the composite elastic response for given set of constituents elastic constants. The finite element software ABAQUS[29] was employed in the calculation.

2.1 Basic model configuration

Through small-angle X-ray scattering measurements, Lin and Argon[1] concluded that in textured nylon 6, obtained by plane-strain channel-die compression to a compression ratio of 3.8 to 4.0, the monoclinic lamellae are straight in the constrained direction (CD) but are S (or arc) shaped with continuously-varying thickness along the loading direction (LD), Fig. 1. For simplicity, a two-dimensional configuration is considered in our calculation. We take a representative layer in the plane of loading direction (LD) and flow direction (FD) (see Fig. 1), on which the alternating crystalline and amorphous, wavy-shaped monoclinic lamellae are exposed. The basic configuration used in this study is shown in Fig. 2, where 1-direction is the loading direction and 2 the flow direction (note this is different from the coordinate system used by Lin and Argon[1]).

The wavy monoclinic lamellae are approximated by sine curves. The middle part of the model is the alternating crystalline and amorphous, monoclinic lamellae. The crystallinity of the lamellae is 43.4% which is the same as the experimentally measured value for a compression ratio of 4.0 by Lin and Argon[1]. For the convenience of computation, the model is filled up to a rectangular shape. Following the arguments of self-consistent method, the elastic property of the filled

portion (top and bottom regions of the model) is taken to be the composite property from Lin and Argon's experimental measurement[1]. The finite element mesh for this model is shown in Fig. 3. Plane strain 8-node biquadratic elements with reduced integration points are used. Theory of small deformation is employed in the calculation.

It was found that nylon 6 crystals in the textured material were predominantly in monoclinic α form, and its (200) planes are statistically-equally divided and oriented with their normals in the directions of $\pm 21^{o}$ with respect to the constrained direction. Therefore, the elastic property of the crystalline part in textured nylon 6 is orthotropic with principal directions along LD, FD and CD. On the other hand, the amorphous part has a transverse isotropic elastic property with its symmetry axis normal to the plane of lamellae. Since the principal axes of the crystalline and the amorphous parts coincide, the lamellae elastic response exhibits orthotropic symmetry with 9 independent elastic constants, as was shown by Lin and Argon's measurements[1]. In the current study, the elastic response of the crystalline part is assumed to obey Hooke's law, as

$$\begin{bmatrix} \varepsilon_{11} \\ \varepsilon_{22} \\ \varepsilon_{33} \\ 2\varepsilon_{23} \\ 2\varepsilon_{31} \\ 2\varepsilon_{12} \end{bmatrix} = \begin{bmatrix} S^c_{11} & S^c_{12} & S^c_{13} & 0 & 0 & 0 \\ S^c_{12} & S^c_{22} & S^c_{23} & 0 & 0 & 0 \\ S^c_{13} & S^c_{23} & S^c_{33} & 0 & 0 & 0 \\ 0 & 0 & 0 & S^c_{44} & 0 & 0 \\ 0 & 0 & 0 & 0 & S^c_{55} & 0 \\ 0 & 0 & 0 & 0 & 0 & S^c_{66} \end{bmatrix} \begin{bmatrix} \sigma_{11} \\ \sigma_{22} \\ \sigma_{33} \\ \sigma_{23} \\ \sigma_{31} \\ \sigma_{12} \end{bmatrix}, \tag{1}$$

where S^c_{ij} are the components of compliance matrix of the crystalline part with 9 independent components, σ_{ij} and ε_{ij} are stress and strain components, respectively. Whereas the elastic response of the amorphous part obeys

$$\begin{bmatrix} \varepsilon_{11} \\ \varepsilon_{22} \\ \varepsilon_{33} \\ 2\varepsilon_{23} \\ 2\varepsilon_{31} \\ 2\varepsilon_{12} \end{bmatrix} = \begin{bmatrix} S^a_{11} & S^a_{12} & S^a_{13} & 0 & 0 & 0 \\ S^a_{12} & S^a_{22} & S^a_{12} & 0 & 0 & 0 \\ S^a_{13} & S^a_{12} & S^a_{11} & 0 & 0 & 0 \\ 0 & 0 & 0 & S^a_{66} & 0 & 0 \\ 0 & 0 & 0 & 0 & 2(S^a_{11} - S^a_{13}) & 0 \\ 0 & 0 & 0 & 0 & 0 & S^a_{66} \end{bmatrix} \begin{bmatrix} \sigma_{11} \\ \sigma_{22} \\ \sigma_{33} \\ \sigma_{23} \\ \sigma_{31} \\ \sigma_{12} \end{bmatrix}, \tag{2}$$

where the number of independent components is 5 for the transverse isotropic symmetry. The stiffness matrices can be obtained by inverting the compliance matrices. For the plane strain deformation considered here, the constants S^c_{44}, S^c_{55} of the crystalline part and $S^a_{44} = S^a_{66}$, $S^a_{55} = 2\,(S^a_{11} - S^a_{13})$ of the amorphous part will not affect the in-plane elastic response. Therefore, they can not be determined by the current simulation. A complete three-dimensional analysis must be performed to obtain these constants, though S^a_{44} and S^a_{55} are not independent material constants in this case.

To obtain the composite elastic constants, three different loadings are applied: plane strain tension in 1 direction, σ^{∞}_{11}; plane strain tension in 2 direction, σ^{∞}_{22}; and a simple shear stress, σ^{∞}_{12}. In all three cases, the magnitude of the applied stress is 1 MPa which is well within the elastic range for this material (typical yield strength of this material is found to be 15-30 MPa). The deformation under this stress level is small enough so that linear theory is adequate. To calculate the global strains corresponding to the applied stresses, the average strain is calculated using the average displacements at the edges of the mesh. For the tensile loadings, to avoid the distortion caused by the wavy lamellae, the displacements of the nodes on the edges (Fig. 3) are constrained such that the nodes on the left edge and that on the right edge have the same respective displacements in 1-direction, whereas those on the top and bottom edges have the same respective displacements in 2-direction.

2.2 Typical finite element result

In order to check whether the wavy shaped finite element mesh has any effects on the numerical results for even a homogeneous media, we first assigned the elastic property of the composite (experimentally measured values) to all elements, and calculated the global elastic response. The results show that the wavy mesh has no effects on the behavior of a homogeneous material. The elastic property of individual elements can be completely recovered at the global level.

For a composite consisting crystalline and amorphous parts, typical deformed finite element mesh under the applied tensile and shear stresses are shown in Figs. 4a-4c. The solid lines represent the displaced mesh, and the broken lines are the original mesh before deformation. To visual-

ize the deformation more clearly, the displacements in the plots are magnified by a factor of 5. It is clear from the figures that, to a crude approximation, the deformations under the tensile stresses are rather uniform throughout the whole body; but the deformation under the shear stress is not very uniform.

The stress and strain distributions within the lamellae are rather complicated due to the nature of the wavy lamellae morphology. Fig. 5 shows the von Mises equivalent stress σ_e distribution under globally applied σ_{11}^{∞}. It is noted that even under the uniform global tensile stress, there will be substantial shear stresses in the lamellae. The equivalent stress can be as high as 4.5 MPa at some locations in the crystalline part, although the applied far field stress is only 1 MPa. This feature will no doubt affect the plastic resistance of semi-crystalline polymers. We will discuss it further later in this paper.

III. Optimization Techniques

As we mentioned before, the objective of this work is to find the set of elastic constants for crystalline and amorphous parts which will result in the same composite elastic response as that measured by Lin and Argon[1]. During the calculation, for each step, the elastic constants of the crystalline and the amorphous part are modified, the resulted elasticity matrix of the composite will be evaluated which, for our plane strain configuration, yields four components of the stiffness matrix: C_{11}, C_{12}, C_{22}, and C_{66}. The following objective function is then constructed to measure the "closeness" between the simulated elastic response and the experimentally measured elastic response of semi-crystalline nylon 6,

$$F(C_{11}, C_{12}, C_{22}, C_{66}) = (C_{11} - C_{11}^e)^2 + (C_{12} - C_{12}^e)^2 + (C_{22} - C_{22}^e)^2 + (C_{66} - C_{66}^e)^2, \quad (3)$$

where C_{11}^e=12.7733 GPa, C_{12}^e=12.4236 GPa, C_{22}^e=19.0171 GPa, and C_{66}^e=0.51125 GPa are experimentally measured values which are listed in Table 1. Apparently, the objective now becomes to search for the constituent elastic constants which minimize the function F, which is a typical multi-variable optimization problem.

For the plane strain problem, the variables to be optimized are the components of compli-

ance matrix for crystalline part S_{ij}^c (except S_{44}^c and S_{55}^c) and the components of compliance matrix for amorphous part S_{ij}^a. In our calculation, the initial values of the elastic constants for the crystalline part are taken from the theoretical calculation by Tashiro and Tadakoro[8]. The initial values of the elastic constants S_{11}^a and S_{22}^a are taken from the experimental measurement by Prevorsek et al.[30], and the initial values of the elastic constants S_{12}^a, S_{13}^a and S_{66}^a are taken from the measurement by Lin and Argon[1] on the textured material. The value of S_{22}^a (measured by Prevorsek et al.[30]) is fixed during optimization (if none of the components is fixed, the obvious optimized values would be that both crystalline and amorphous parts possess the composite property, leading to a zero minimum error for function F), thus the total number of variables is 11 in this optimization problem.

For each step of optimization, the condition of non-negative elastic strain energy requires that the elasticity matrices must be positive-definite. In other words, all components of the stiffness matrices must be larger than or equal to zero; the diagonal components of the compliance matrices must be positive, whereas the off-diagonal components of the compliance matrices must be less than or equal to zero. These requirements highly restrict the application of conventional optimization methods based on gradient vectors or Hessian matrices. For this specific optimization problem, we find that Powell's direct search method[31], which makes use of the function values directly without calculating their derivatives, is preferred. By searching in the directions which are mutually conjugate (according to Powell' optimization scheme[31]), the objective function F has been minimized successfully.

The values of the objective function F as a function of step numbers is plotted in Fig. 6. The value decreases rapidly at the beginning, and levels off gradually. The final value of F is about 0.68% of the initial value based on the initial guess of constituent elastic constants.

IV. Results and Discussion

The calculated values of the four composite elastic constants, C_{11}, C_{12}, C_{22}, and C_{66} for two-dimensional configuration using the optimized constituent elastic properties are given in Table 1, along with the experimental results by Lin and Argon[1]. Three of our calculated elastic

constants, C_{11}, C_{12}, and C_{22}, match Lin and Argon's experimental data very well. Only the shear component C_{66} differs from the experimental results with a high percentage error. The experimental data shows a much lower shear resistance of the materials than the calculation prediction. It is also noted that the shear modulus of textured nylon 6 is more than one order of magnitude lower than the corresponding Young's modulus. The material is very "soft" in shear. With the objective function defined in (3), the error sensitivity is based on the absolute error, so it is not very sensitive to the relatively small quantities percentage-wise. Nevertheless, if we take a relative error for each component as the percentage of the experimental data, X, as,

$$X = \frac{|C_{11} - C_{11}^e|}{C_{11}^e} = \frac{|C_{22} - C_{22}^e|}{C_{22}^e} = \frac{|C_{12} - C_{12}^e|}{C_{12}^e} = \frac{|C_{66} - C_{66}^e|}{C_{66}^e}, \tag{4}$$

the objective function for a uniform percentage error, X, would be given as,

$$F(C_{11}, C_{12}, C_{22}, C_{66}) = 679.6X^2. \tag{5}$$

Compare with the final value of function F obtained by our calculation, our relative error is equivalent to an "across-the-board" percentage error of 5.66% when compared to the experimental measurements of Lin and Argon[1]. Considering the experimental scattering (see Lin's thesis[32]), this average percentage error is considered very acceptable.

Table 1 also shows the experimental data of elastic constants measured by Leung et al.[33] at about 25°C (we should point out that in Table IV of Lin and Argon[1], the data of Leung et al.[33] at a different temperature, -40°C, were quoted). Our simulated elastic constants are generally higher than their data. This could be attributed to two factors. First, the crystallinity of their textured material is 39.2% whereas we used 43.3% in our simulation. This partly explains why our material is stiffer than theirs because higher crystallinity usually results in higher tensile elastic resistance, although not necessarily higher shear resistance. Second, their textured material was obtained by uniaxial drawing, thus possesses a different morphology. Their material is transverse isotropic with symmetry axis along the drawing direction (flow direction). Therefore, direct comparison of these two results is somewhat misleading.

However, if a complete three dimensional analysis were performed, we would be able to predict the transverse isotropic behaviors using the complete set of nine elastic constants for crystalline part and 5 elastic constants for amorphous part for a given morphology. Although this

information is not known, we can still use the nine elastic constants for textured orthortropic nylon 6 obtained by Lin and Argon[1] to estimate the five elastic constants of the corresponding transverse isotropic material obtained by uniaxial drawing as that by Leung et al[33]. We performed a simple analysis to convert the orthortropic material behavior to a transverse isotropic property. The basic assumption here is that the lamellae are randomly oriented in the plane normal to the drawing direction (flow direction), thus the density of (200) and (002) planes along any direction normal to the drawing direction must be the same. Based on this argument, the five elastic constants of the transverse isotropic material were obtained using the nine constants from Lin and Argon[1] for orthortropic material. Detailed derivations which make use of coordinate transformation and averaging techniques are given in the Appendix. The resulted five compliance components are listed in Table 2 and compared with the results by Leung et al.[33] at 25°C (We should also point out that the compliance components calculated in Leung et al.[33] from the stiffness matrix were not very accurate. We re-calculated them to make sure that the compliance matrix is the inverse of the stiffness matrix). The agreement is surprisingly good. Considering the fact that the crystallinity of textured material by Lin and Argon[1] is slightly higher than that by Leung et al.[33] (43.3%[1] vs. 39.2%[33]), the slightly lower values of tensile compliances and the slightly higher value of shear compliance of Lin and Argon's results are exactly what we should expect.

The compliance components for crystalline part which minimize the objective function are given in Table 3. Column 2 and 3 of Table 3 are the theoretically calculated values by Tashiro and Tadokoro[8] and experimentally measured values from the crystalline regions by Sakurada and Kaji[34], respectively. Our simulation results of the compliance components are consistently lower than those measured by Sakurada and Kaji[34], which indicates that the crystalline part is stiffer in both loading and flow directions than the material tested by them. Compared to the theoretical calculation by Tashiro and Tadokoro[8], our results have the same trend as that predicted by them, although the numerical values are different. The prediction of the compliance in loading direction S_{11}^c by our simulation is lower than their theoretical calculation (more stiff), whereas the compliances in flow direction (chain direction) and constrained directions are higher than the theoretical calculation (softer). More noteworthy is the shear compliance for which our simulated value is lower than the theoretical calculation by a factor of more than 2. Our simulation results for both

crystalline S_{66}^c and amorphous S_{66}^a seem to be rather low. It is unclear to us what the reason could be for this discrepancy.

The optimal values of the compliances of the amorphous part are given in Table 4. Since we used the experimental data of Prevorsek et al.[30] for S_{22}^a as the given datum, we did not consider this compliance component as variable during our simulation. As expected, the compliances of the amorphous part S_{11}^a, S_{22}^a and S_{33}^a are notably higher than the corresponding components of the crystalline part. But the shear compliance S_{66}^a is lower than the corresponding compliance for crystalline part S_{66}^c, indicating that the entangled chains in amorphous part can provide more resistance to shear deformation than the well aligned chains with predominantly Van der Waals bonding between them in the crystalline part.

V. Concluding Remarks

In this study we have obtained the elastic constants of the constituents of semi-crystalline nylon 6, crystalline part and amorphous part, by computer simulation of a known morphology of the material. In principle, we could apply this technique to study the two important effects in polymer deformations, temperature effect and humidity effect, on the crystalline part and the amorphous part respectively, provided their effects on semi-crystalline nylon 6 are known. The complete understanding of the individual behavior of the crystalline and amorphous parts over a range of temperature and humidity will provide a powerful tool for predicting the behaviors of real engineering polymeric materials.

It is easy to note that the application of this technique is not limited to nylon 6. It can be applied to any semi-crystalline polymeric material provided the morphology of that material is known. Furthermore, sensitivity of mechanical response of semi-crystalline polymers to microscopic morphological variations can also be easily investigated by this technique.

In addition to estimating the elastic properties of individual constituents of semi-crystalline polymers, this technique can also be used to study plastic resistance of the material and estimate the critical resolved shear stress. It is noted in Fig. 5 that because of the wavy morphology in textured nylon 6, the von Mises equivalent stress at some locations could be 4 to 5 times higher than

the applied far field stress. Like in any composite materials, higher stresses always occur in an elastically stiffer constituent which, in our case, is the crystalline part. This stress concentration will result in an apparently lower yield strength of the material, thus result in an underestimate of critical resolved shear stresses.

Acknowledgment

The authors are very grateful to Prof. A.S. Argon for suggesting the problem to us. KJH and YX were partially supported by the University of Illinois. KJH was also partially supported by NSF under Grant MSS 92-09309. LL was supported by DARPA through the Office of Naval Research under contract N00014-86-K-0768. The computation was partially supported by National Center for Supercomputing Applications under Grant No. TRA920139N and utilized the CRAY Y-MP4/464 at the NCSA, University of Illinois at Urbana-Champaign.

References

(1) Lin, L.; Argon, A.S. *Macromolecules* **1992** *25*, 4011.

(2) Lewis, E.L.V.; Ward, I.M. *J. Polym. Sci., Polym. Phys. Ed.* **1989**, *27*, 1357.

(3) Choy, C.L.; Leung, W.P.; Ong, E.L. *J. Polym. Sci., Polym. Phys. Ed.* **1988**, *26*, 1569.

(4) Ward, I.M. *Mechanical Properties of Solid Polymers*, 2nd Ed., Wiley-Interscience, New York, **1985**.

(5) Lin, L.; Argon, A.S. "Structure and Plastic deformation of Polyethylene (A Review)", *J. Mater. Sci.*, submitted for publication.

(6) Born, M.; Huang, T. *Dynamical Theory of Crystal Lattices*, Clareendon Press, Oxford, **1956**.

(7) Tashiro, K.; Kobayashi, M.; Tadokoro, H. *Macromolecules* **1978**, *11*, 908.

(8) Tashiro, K.; Tadokoro, H. *Macromolecules* **1981**, *14*, 781.

(9) Clements, J.; Jakeways, R.; Ward, I.M. *Polymer* **1978**, *19*, 639.

(10) Sakurada, I.; Kaji, K. *Makromol. Chem., Suppl.* **1975**, *1*, 599.

(11) Sakurada. I.; Ito, T.; Nakamae, K. *J. Polym. Sci., Part C* **1966**, *15*, 75.

(12) Prevorsek, D. C.; Kwon, Y.D.; Sharma, R.K. *J. Mater. Sci.* **1977**, *12*, 2310.

(13) Faraday Disc. of Chem. Soc., 1979, vol. 68.

(14) Ward, I.M. *Proc. Phys. Soc.* **1962**, *80*, 1176.

(15) Allison, S.W.; Ward, I.M. *Brit. J. Appl. Phys.* **1967**, *18*, 1151.

(16) Gupta, V.B.; Ward, I.M. *J. Macromol. Sci., B* **1967**, *1*, 373.

(17) Takayanagi, M.; Imada, K.; Kajiyama, T. *J. Polym. Sci., C* **1966**, *15*, 263.

(18) Lewis, E.L.V.; Ward, I.M. *J. Macromol. Sci., Phys.* **1980**, *B18*, 1.

(19) Halpin, J.C.; Kardos, J.L. *J. Appl. Phys.* **1972**, *43*, 2235.

(20) Kardos, J.L.; Raisoni, J. *Polym. Eng. Sci.* **1975**, *15*, 183.

(21) Wang, T.T. *J. Appl. Phys.* **1973**, *44*, 2218.

(22) Wang, T.T. *J. Appl. Phys.* **1973**, *44*, 4052.

(23) Wang, T.T. *J. Polym. Sci., Polym. Phys. Ed.* **1974**, *12*, 145.

(24) Hill, R. *J. Mech. Phys. Solids* **1964**, *12*, 199; *ibid* **1965**, *13*, 189.

(25) Hermans, J.J. *Proc. K. Ned. Akad. Wet.* **1967**, *B70*, 1.

(26) Kroner, K. *Z. Phys.* **1958**, *151*, 504.

(27) Hershey, A.V. *J. Appl. Mech.* **1954**, *21*, 236.

(28) Kerner, E.H. *Proc. Phys. Soc. Lond.* **1956**, *B69*, 808.

(29) Hibbitt, Karlsson and Sorensen, Inc., ABAQUS Finite Element Software, version 4.9, 1992.

(30) Prevorsek, D.C.; Harget, P.J.; Scharma, R.K. *J.Macromol. Sci.-Phys.* **1973**, *B8*, 127.

(31) Powell, M.J.D. *Compt. J.* **1964**, *7*, 155.

(32) Lin, L. "An Experimental Study of Deformation Mechanisms and Resistances of Semi-Crystalline Polymers", PhD Thesis, Massachusetts Institute of Technology, 1991.

(33) Leung, W.P.; Ho, K.H.; Choy, C.L. *J. Polym. Sci., Polym. Phys. Ed.* **1984**, *22*, 1173.

(34) Sakurada, I.; Kaji, K. *J. Polym. Sci.: Part C* **1970**, *31*, 57.

Table 1: Elastic constants of semi-crystalline nylon 6 (GPa)

	Present Result	Lin and Argon[1]	Leung et al.[33]
C_{11}	12.7527	12.7733	7.4625
C_{12}	11.4107	12.4236	4.9938
C_{22}	19.5862	19.0171	9.900
C_{66}	1.3981	0.51125	1.1813

*Crystallinity of the material used by Lin and Argon[1] is 43.3%.

*Crystallinity of the material used by Leung et al.[33] is 39.2%, test temperature was 25°C.

Table 2: Elastic compliances of transverse isotropic material (GPa^{-1})

	Converted from Lin and Argon[1]	Leung et al.[33]
S_{11}	0.283	0.292
S_{12}	-0.086	-0.066
S_{13}	-0.150	-0.162
S_{22}	0.163	0.167
S_{66}	1.338	0.847

Table 3: Elastic compliances of the crystalline part (GPa^{-1})

	Present Result	Tashiro and Tadadoro[8]	Sakurada and Kaji[34]
S_{11}^c	0.1973	0.3838	0.877
S_{22}^c	0.0395	0.0032	0.061
S_{33}^c	0.1969	0.1234	0.877
S_{12}^c	-0.0166	-0.0010	
S_{13}^c	-.01902	-0.1203	
S_{23}^c	-0.00144	-0.0001	
S_{66}^c	0.2326	0.4195	

*Tashiro and Tadadoro's values[8] are theoretically calculated.

Table 4: Elastic compliances of the amorphous part (GPa^{-1})

	Prevorsek et al.[30]	Present Result
S_{11}^a	1.430	1.420
S_{22}^a	0.427	0.427
S_{33}^a	1.430	1.420
S_{12}^a		-0.4843
S_{13}^a		-0.080
S_{23}^a		-0.4843
S_{66}^a		0.1409

Appendix

The nine elastic compliances for an orthorhombic material are known as,

$$\begin{bmatrix} S_{11} & S_{12} & S_{13} & 0 & 0 & 0 \\ S_{12} & S_{22} & S_{23} & 0 & 0 & 0 \\ S_{13} & S_{23} & S_{33} & 0 & 0 & 0 \\ 0 & 0 & 0 & S_{44} & 0 & 0 \\ 0 & 0 & 0 & 0 & S_{55} & 0 \\ 0 & 0 & 0 & 0 & 0 & S_{66} \end{bmatrix}, \tag{A1}$$

where the compliance components S_{mn} are related to compliance tensor S_{ijkl} by

$$S_{11} = S_{1111}, S_{12} = S_{1122}, S_{13} = S_{1133}, S_{22} = S_{2222}, S_{23} = S_{2233}, S_{33} = S_{3333},$$
$$S_{44} = 4S_{2323}, S_{55} = 4S_{3131}, S_{66} = 4S_{1212}. \tag{A2}$$

In order to obtain the transverse isotropic material property with its symmetry axis along the chain direction, we assume that the lamellae orientation distribution in the plane normal to the chain direction (1-3 plane in our case) is random. Thus the density of any specific orientation, $f(\theta)$, is uniform over the range of θ=0--2π in the isotropic plane (see Fig. 7 for definition of θ), and can be given by

$$f(\theta) = \frac{1}{2\pi}. \tag{A3}$$

Then the new transverse isotropic compliance matrix $[S_{mn}']$ is obtained by integrating the orthorhombic compliance matrix over 2π in the plane normal to the symmetry axis, as

$$[S_{mn}'] = \int_0^{2\pi} f(\theta)\,[S_{m'n'}(\theta)]\,d\theta, \tag{A4}$$

where $[S_{m'n'}(\theta)]$ is the compliance matrix of lamellae with orientation along θ direction. The tensor coordinate transformation is used to obtain $[S_{m'n'}(\theta)]$, such that,

$$S_{i'j'k'l'} = l_{i'i}l_{j'j}l_{k'k}l_{l'l}S_{ijkl}, \tag{A5}$$

where $l_{i'j}$'s are direction cosines between i' and j axes, and i, j, k, l = 1,2,3.

For the configuration we are considering, i.e., the 1-3 plane as the isotropic plane, we have, upon performing the integration (A4),

$$S_{11}' = S_{33}' = \frac{3}{8}(S_{11} + S_{33}) + \frac{1}{4}S_{13} + \frac{1}{8}S_{55} \tag{A6.1}$$

$$S_{22}' = S_{22} \tag{A6.2}$$

$$S_{12}' = S_{23}' = \frac{1}{2}(S_{23} + S_{12}) \tag{A6.3}$$

$$S_{13}' = \frac{1}{8}(S_{11} + S_{33}) + \frac{3}{4}S_{13} - \frac{1}{8}S_{55} \tag{A6.4}$$

$$S_{44}' = S_{66}' = \frac{1}{2}(S_{44} + S_{66})\,. \tag{A6.5}$$

Using the values of the orthorhombic compliances by Lin and Argon[1], we obtained the five elastic compliances for a transverse isotropic material which are given in Table 2.

Figure Captions

Fig. 1 Morphology of textured nylon 6 after deep channel-die compression to a compression ratio of 3.8 to 4.0: a) Lamellae orientations; b) Lattice orientations.

Fig. 2 Model used in the current study showing the alternative crystalline and amorphous parts in the middle, and the composite to fill up the rectangular configuration.

Fig. 3 The finite element mesh of this model.

Fig. 4 The deformed finite element meshes under: a) plane strain tension along loading direction σ_{11}^{∞}; b) plane strain tension along flow direction σ_{22}^{∞}; and c) simple shear σ_{12}^{∞}.

Fig. 5 Contours of von Mises equivalent stress σ_e under far field tensile stress σ_{11}^{∞}.

Fig. 6 Values of the objective function F after different steps of optimization.

Fig. 7 Conversion from an orthorhombic material to a transverse isotropic material: a) orthorhombic semi-crystalline material; b) orientation of a specific lamellae with respect to global coordinate system.

(a)

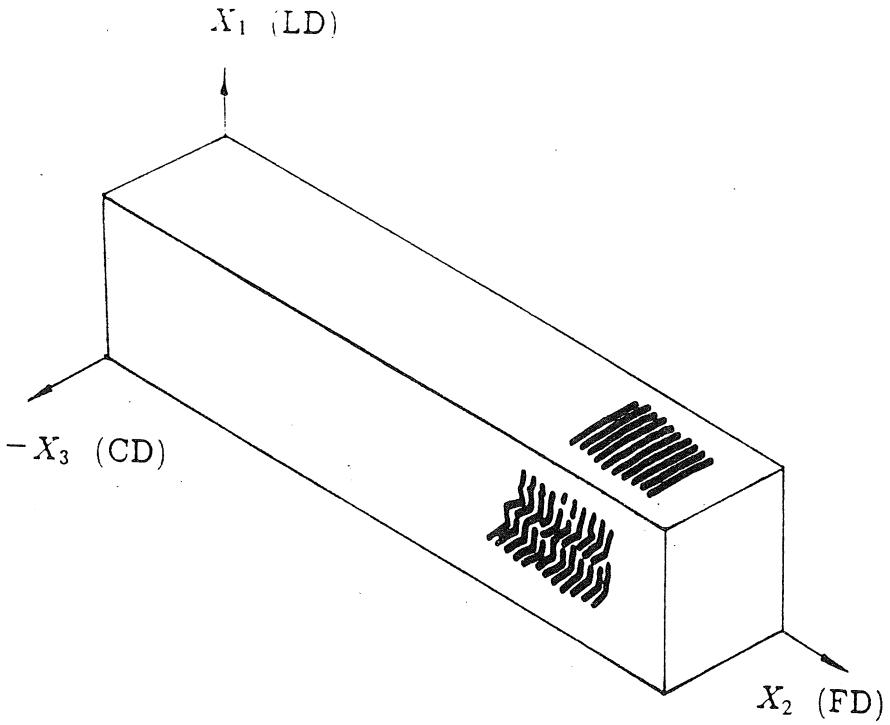
X_1 (LD)
$-X_3$ (CD)
X_2 (FD)

(b)

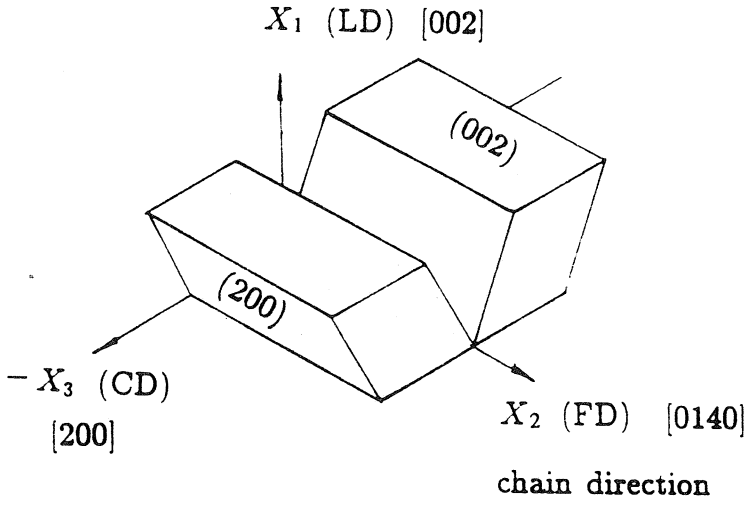
X_1 (LD) [002]
(002)
(200)
$-X_3$ (CD)
[200]
X_2 (FD) [0140]
chain direction

Figure 1

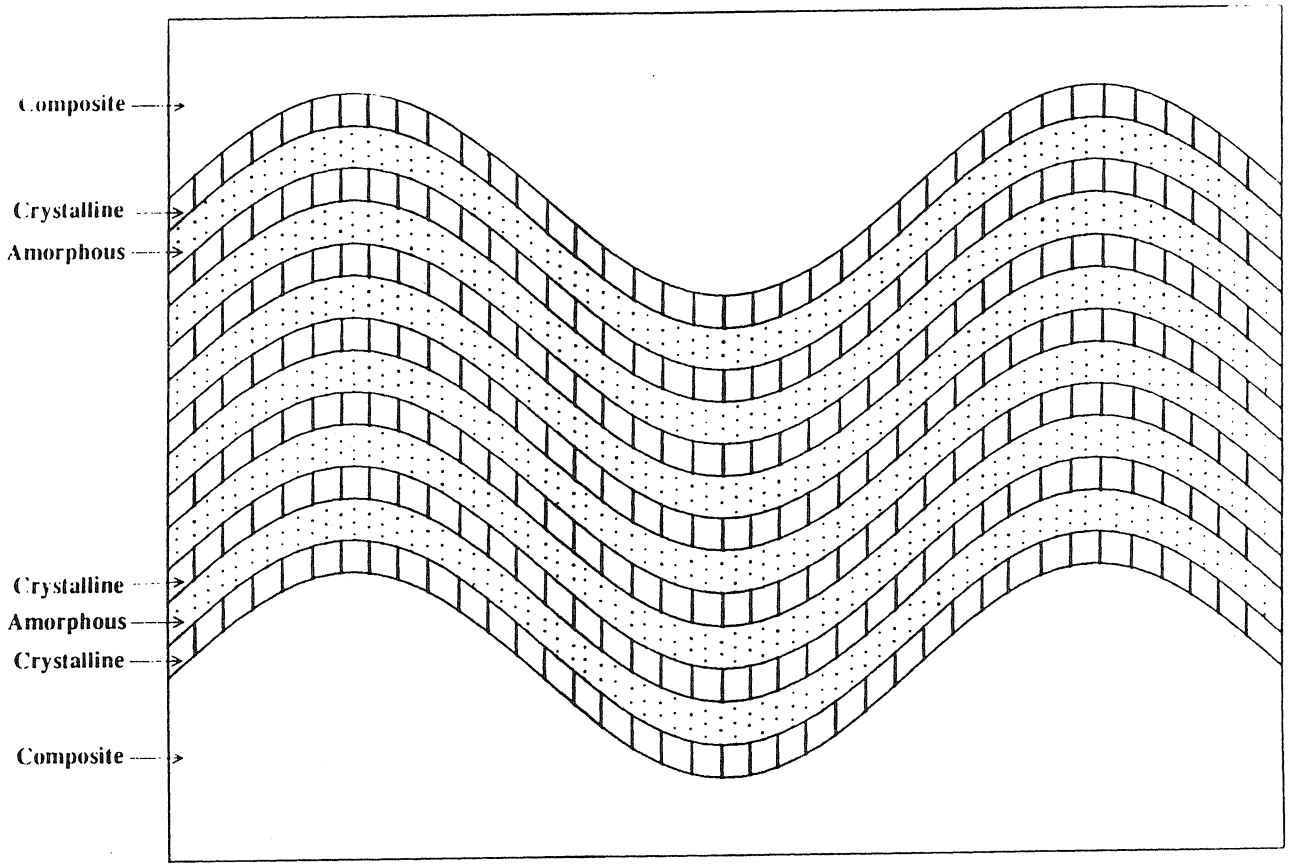
Composite
Crystalline
Amorphous
Crystalline
Amorphous
Crystalline
Composite

Figure 2

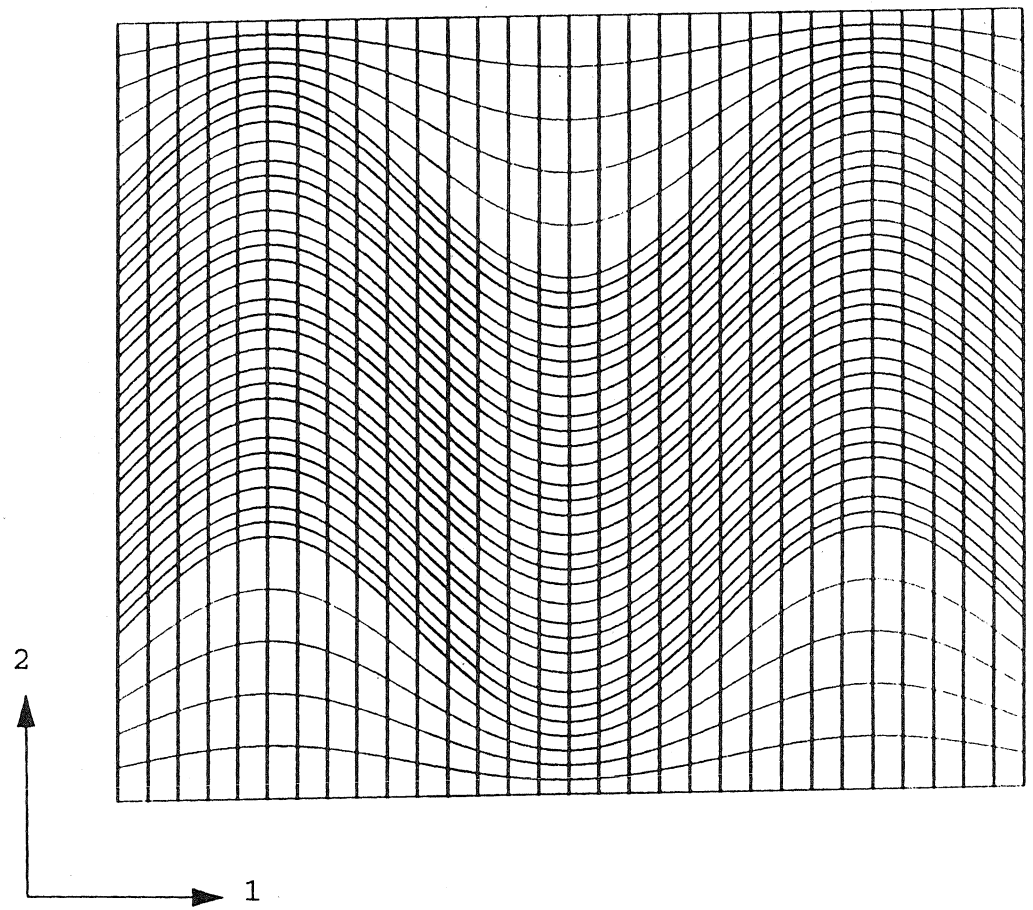

Figure 3

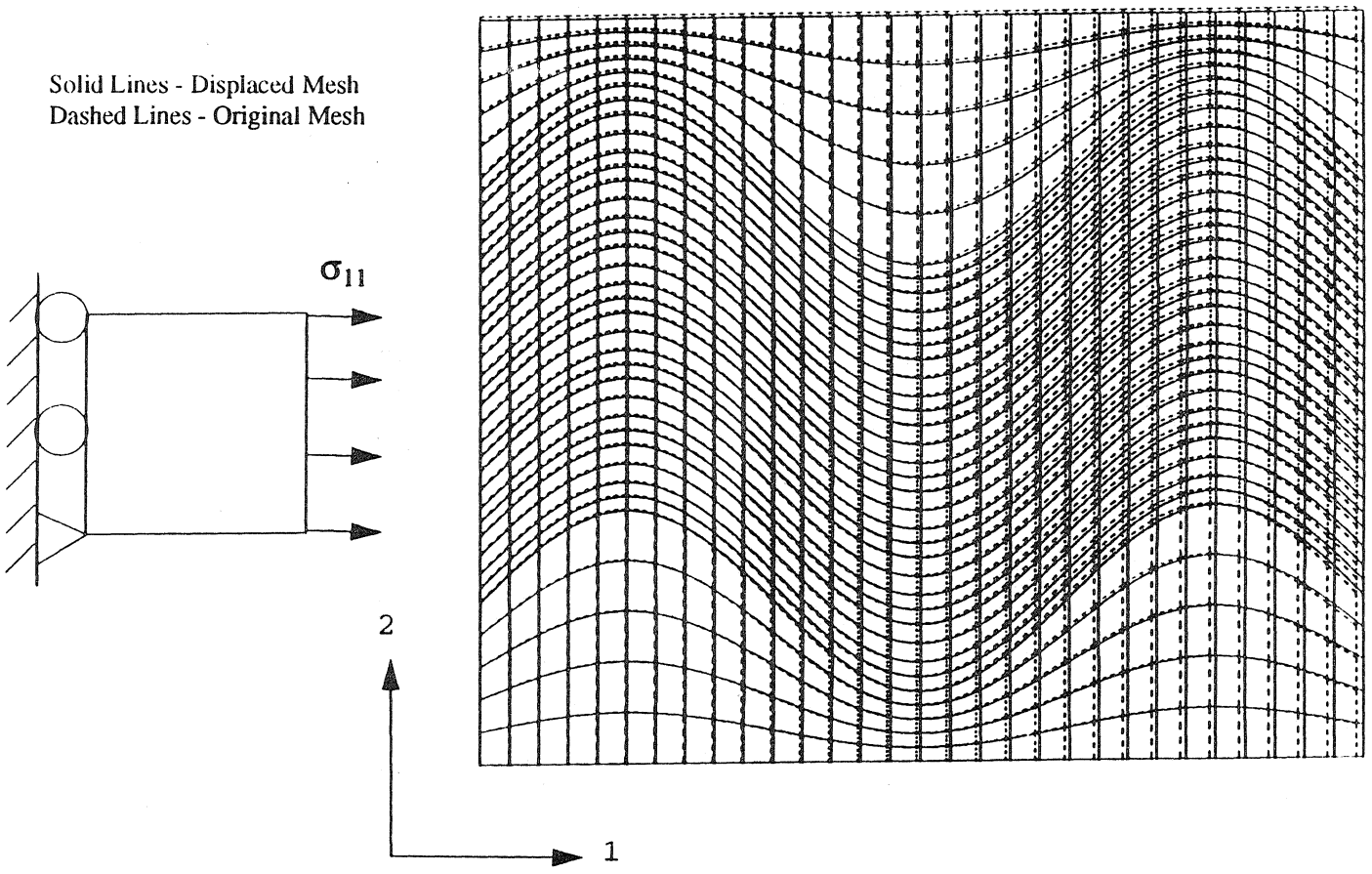
Solid Lines - Displaced Mesh
Dashed Lines - Original Mesh
σ_{11}
2
1

Figure 4a

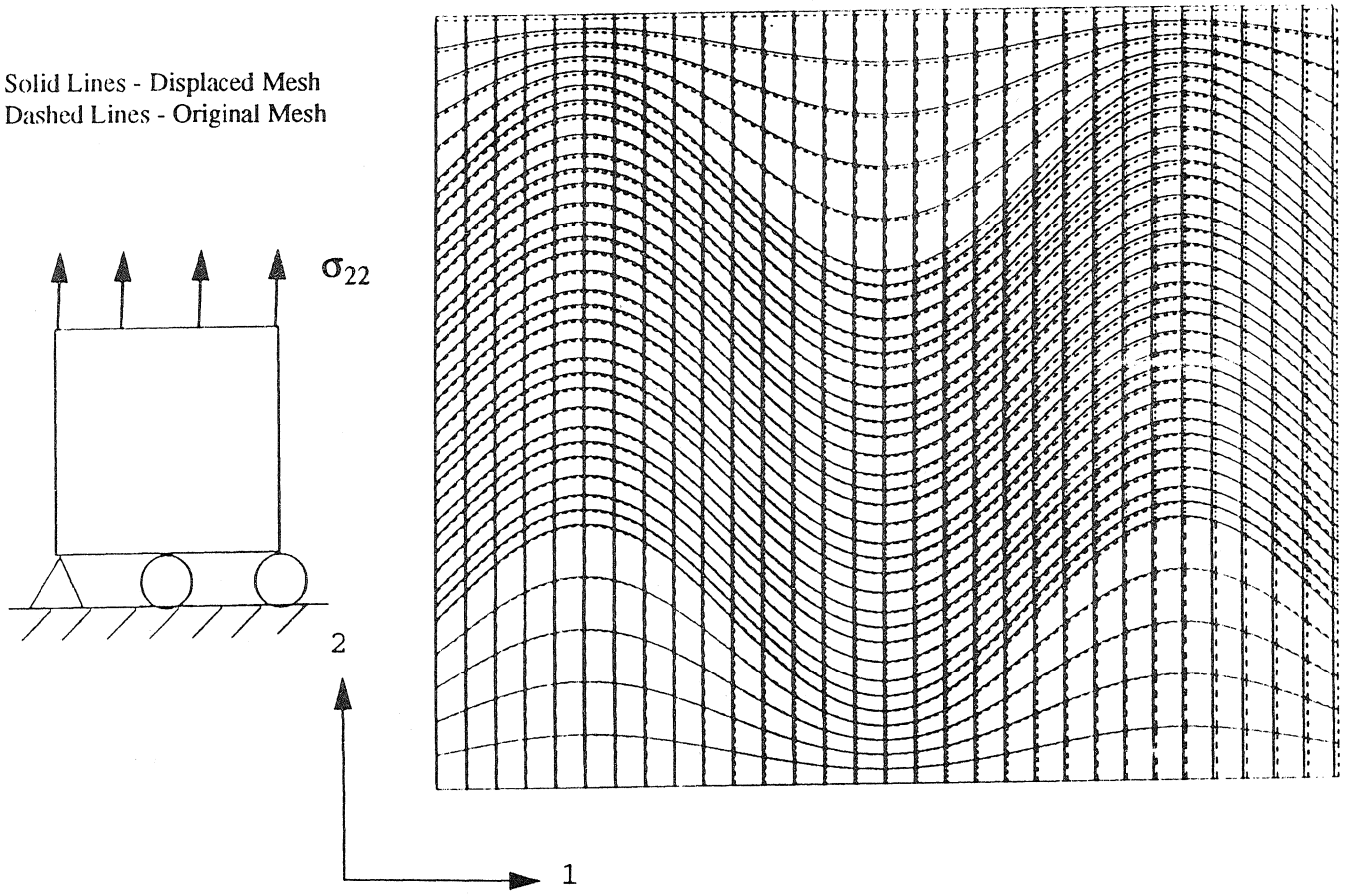
Solid Lines - Displaced Mesh
Dashed Lines - Original Mesh
σ22
2
1

Figure 4b

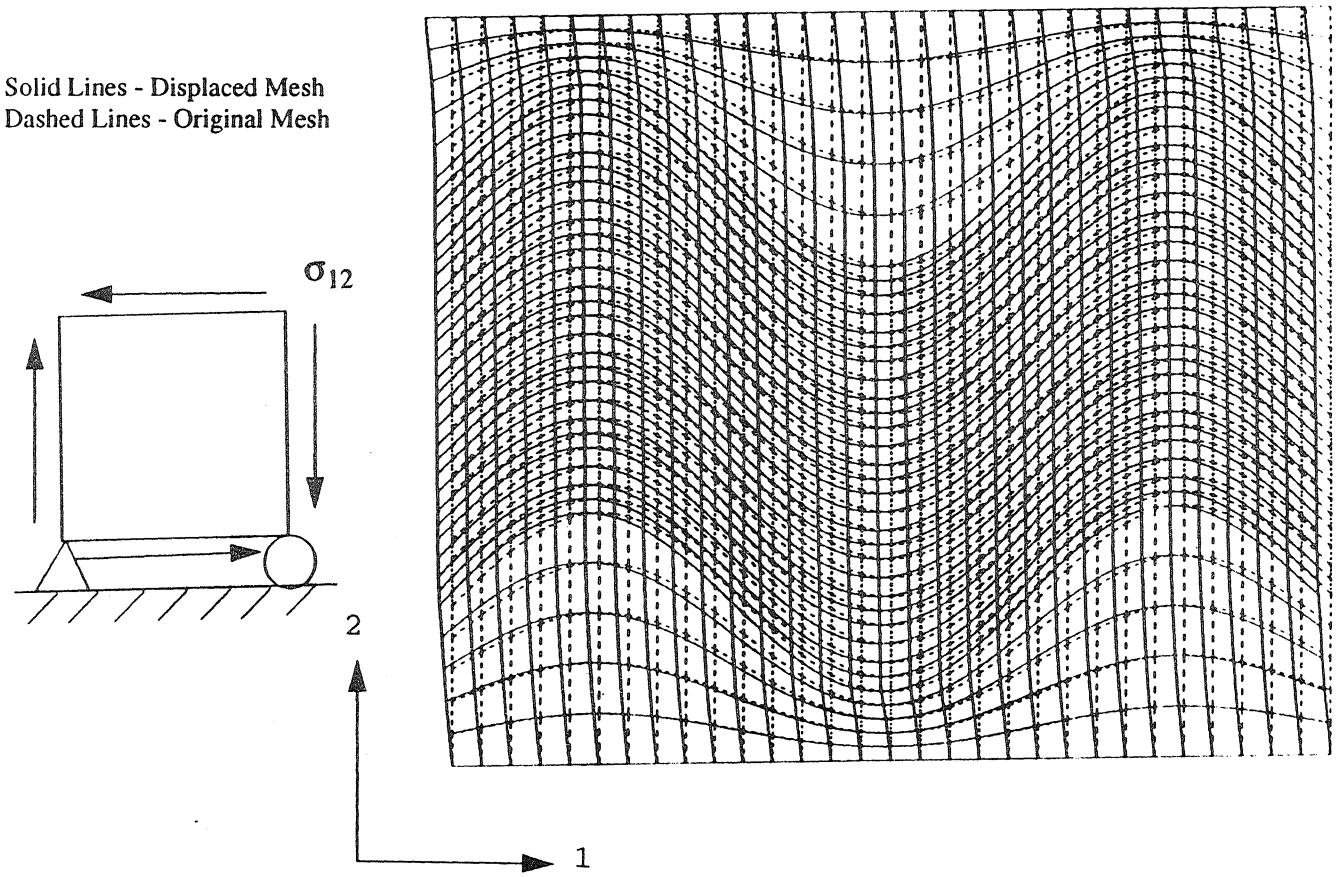
Solid Lines - Displaced Mesh
Dashed Lines - Original Mesh
σ12
2
1

Figure 4c

von Mises Stress

Contour No.	Values(MPa)
1	0.0
2	0.9
3	1.8
4	2.7
5	3.6
6	4.5
7	5.4
8	6.3
9	7.2
10	8.1
11	9.0

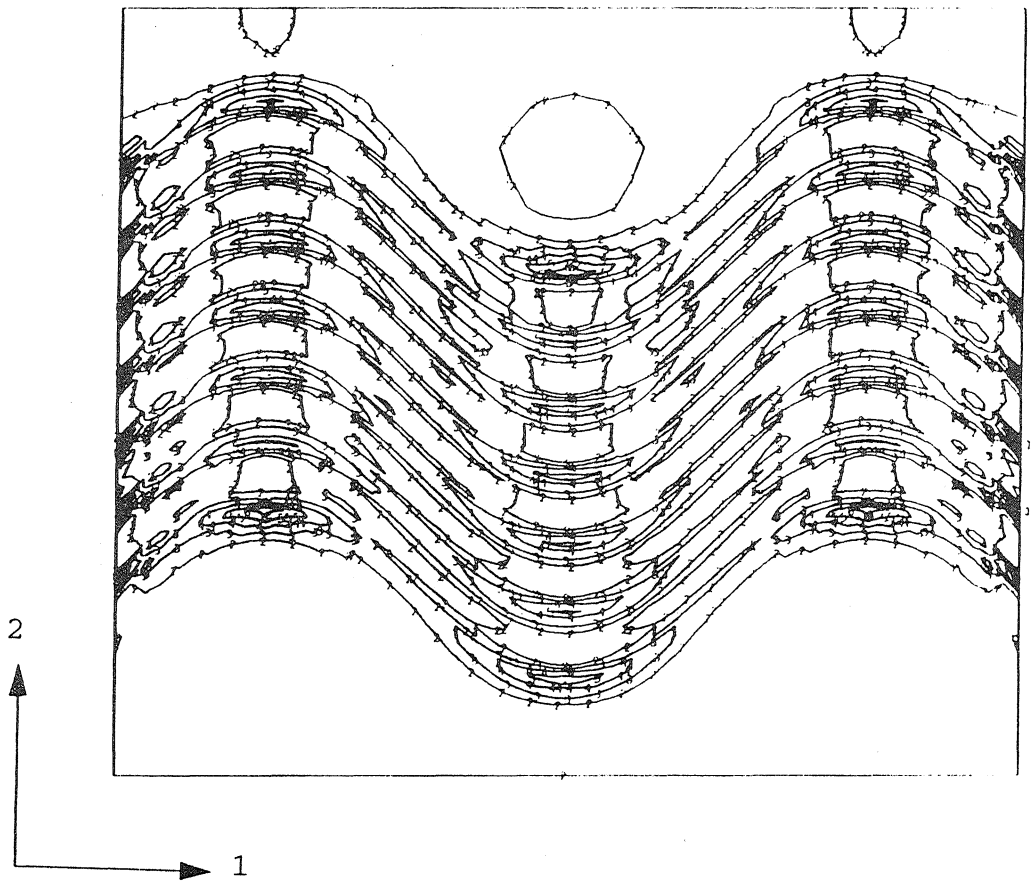

Figure 5

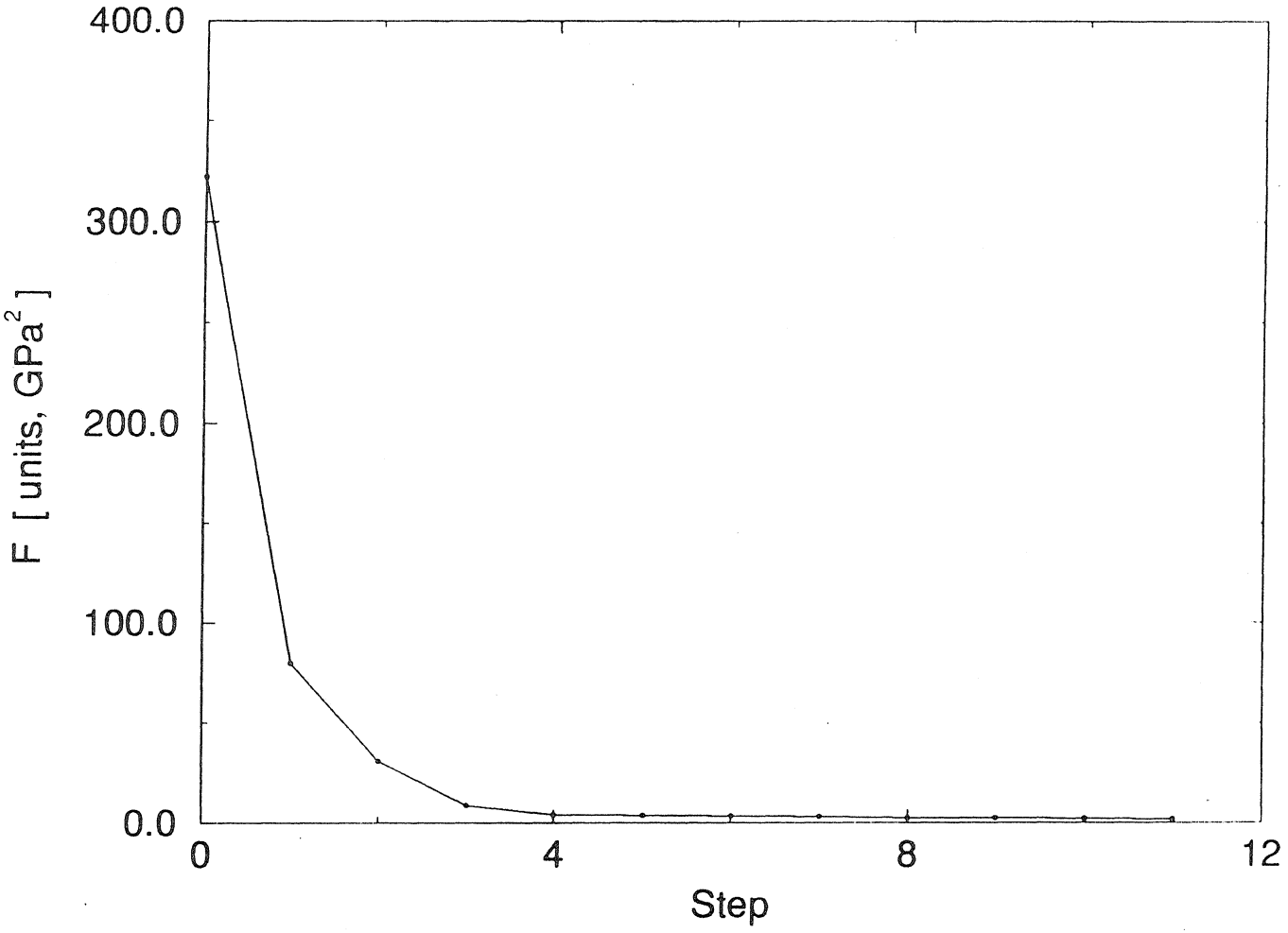

Figure 6

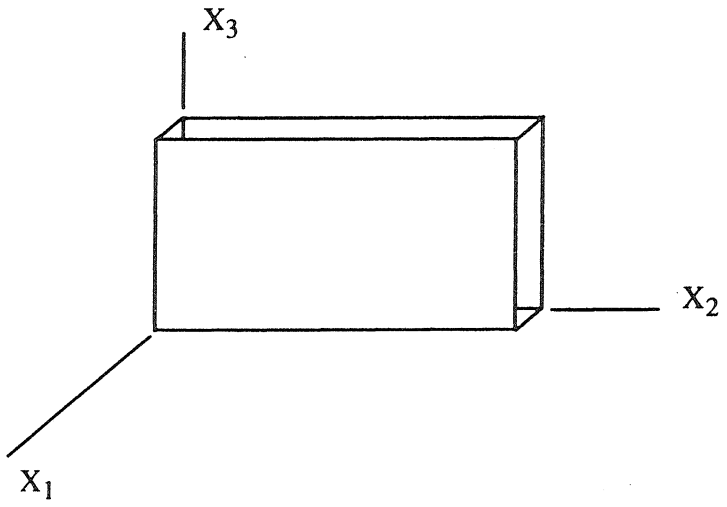

(a)

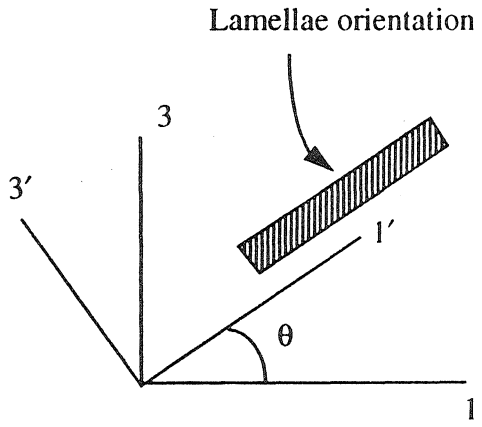

(b)

Figure 7